Geophysical constraints on the properties of a subglacial lake in northwest Greenland

Ross Maguire[1,2], Nicholas Schmerr[1], Erin Pettit[3], Kiya Riverman[4], Christyna Gardner[5], Daniella N. DellaGiustina[6], Brad Avenson[7], Natalie Wagner[8], Angela G. Marusiak[1], Namrah Habib[6], Juliette I. Broadbeck[6], Veronica J. Bray[6], Samuel H. Bailey[6]

[1]Department Geological Sciences, University of Maryland, College Park MD, 20742, USA
[2]Department of Earth and Planetary Sciences, University of New Mexico, Albuquerque NM, 87131, USA
[3]College of Earth, Ocean, and Atmospheric Sciences, Oregon State University, Corvallis OR, 97331-5503, USA
[4]Courant Institute of Mathematical Sciences, New York University, New York NY 10012 USA
[5]Department of Geosciences, Utah State University, Logan UT, 84322-4505, USA
[6]Lunar and Planetary Laboratory, University of Arizona, Tucson AZ, 85721-0092, USA
[7]Silicon Audio Inc., Austin TX, USA
[8]Department of Geosciences, University of Alaska, Fairbanks AK, 99775, USA

Correspondence to: Ross Maguire (rmaguire@umd.edu)

Abstract.

In this study, we report the results of an active source seismology and ground-penetrating radar survey performed in northwestern Greenland where Palmer et al. (2013) proposed the presence of a subglacial lake beneath the accumulation area. Both seismic and radar results show a flat reflector approximately 830 - 845 m below the surface, with a seismic reflection coefficient of -0.43 +/- 0.17, which is consistent with the acoustic impedance contrast between a layer of water below glacial ice. Additionally, in the seismic data we observe an intermittent lake bottom reflection arriving between 14 - 20 ms after the lake top reflection, corresponding to a lake depth of approximately 10 - 15 m. A strong coda following the lake top and lake bottom reflections is consistent with a package of lake bottom sediments although its thickness and material properties are uncertain. Finally, we use these results to conduct a first-order assessment of the lake origins using a one-dimensional thermal model and hydropotential modeling based on published surface and bed topography. Using these analyses, we narrow the lake origin hypotheses to either anomalously high geothermal flux or hypersalinity due to local ancient evaporite. Because the origins are still unclear, this site provides an intriguing opportunity for the first *in situ* sampling of a subglacial lake in Greenland, which could better constrain mechanisms of subglacial lake formation, evolution, and relative importance to glacial hydrology.

1 Introduction

There is mounting evidence that subglacial lake systems below the Antarctic and Greenland ice sheet play an important role in glacier dynamics and ice-sheet mass balance considerations. In Antarctica, the presence of subglacial lakes is suspected to promote ice flow by reducing basal shear stress (e.g., Bell et al., 2007), and periodic drainage events have been linked to accelerated ice flow in outlet glaciers and ice streams (e.g., Stearns et al., 2008; Siegfried et al., 2016). Similarly, in Greenland subglacial lake systems also provide a reservoir for the storage of surface or basal melt water, and hence may be an important, but largely unknown, factor in global sea level change. Additionally, subglacial lakes are of interest due to their ability to harbor complex microorganisms adapted to extreme environments (Achberger et al., 2016; Campen et al., 2019; Vick-Majors et al., 2016) and for paleoenvironmental information contained in subglacial lake sediments (Bentley et al., 2011).

While the presence and nature of subglacial lakes underlying the Antarctic ice sheet has been studied for more than 50 years, the existence of subglacial lakes below the Greenland ice sheet is a relatively recent discovery and comparatively little is known about their properties and origin. Detection of subglacial lakes has relied on a variety of methods, including radio-echo sounding (Robin et al., 1970; Siegert et al., 1996; Langley et al., 2011; Palmer et al., 2013; Young et al., 2016; Bowling et al., 2019) satellite altimetry measurements (Fricker et al., 2007; Palmer et al., 2015; Siegfried & Fricker, 2018; Willis et al., 2015), and active source seismic experiments (e.g., Horgan et al., 2012; Peters et al., 2008). Using these techniques, approximately 400 subglacial lakes have been detected in Antarctica (Wright & Siegert, 2012), of which 124 are considered "active" by Smith et al., (2009). In Greenland, subglacial lakes were first detected in radio-echo sounding data by Palmer et al. (2013), who identified two small (roughly 10 km^2) flat regions of anomalously high basal reflectivity below the northwestern Greenland ice sheet. These features, named "L1" and "L2", were discovered below 757 m and 809 m of ice respectively. Recently, Bowling et al. (2019) greatly expanded the inventory of subglacial lakes in Greenland to approximately 54 candidates based on a combination of airborne radio-echo sounding and satellite altimetry data. The new inventory shows that, in contrast to subglacial lakes in Antarctica which tend to form under thick (> 4 km) warm-based ice in the continental interior, the majority of subglacial lakes in Greenland are found under relatively thin (1 - 2 km) ice near the margins of the ice sheet. Bowling et al. (2019) find that most subglacial lakes in Greenland appear to be stable features, showing temporally consistent radio-echo sounding signatures and an absence of vertical surface deformation over the decadal time scales of observation. Of the 54 candidate lakes, only 2 showed signs of vertical surface deformation indicative of active draining or recharge.

The formation and location of the detected subglacial lake features in Greenland remains elusive because many are located in regions where observations and modeling suggest that the base of the ice is frozen to its bed (MacGregor et al., 2016). Complicating our understanding of the nature of subglacial lakes is the fact that uniquely identifying lakes in radar data is challenging since basal reflectivity is sensitive to both the physical properties and the roughness of the material underlying the ice (e.g., Jordan et al., 2017). Amplitude anomalies of radar echoes in the range of +10 to +20 dB are often interpreted as

65   subglacial lakes, although flat regions of saturated sediment may produce similar anomalies. Furthermore, the total volume of water stored in subglacial lake systems is unknown since airborne and space based remote sensing observations are incapable of measuring lake depth (i.e., water column thickness).

    Seismic investigations provide an independent means of confirming the presence of subglacial lakes and are capable of
70   measuring lake depth and underlying geological structures which can provide valuable clues into their formation and total volume. For example, Peters et al., (2008) performed an active source seismic survey near the South Polar region of Antarctica, and observed reflections from both the top and bottom of a subglacial lake that lies 2.8 km below the ice surface, which allowed them to image a lake depth of about 32 m and infer the underlying sedimentary structure. Additionally, Woodward et al., (2010) performed an active source seismic investigation of lake Ellsworth in west Antarctica, which lies at the bottom of a
75   narrow subglacial valley below approximately 3 km of ice. They found large variations in lake depth from between 52 m to 156 m and were able to estimate the total volume of liquid water to be 1.37 km^3. Later, Smith et al., (2018) reanalyzed the data to investigate the sedimentary structure below lake Ellsworth, and found evidence of a thin sedimentary package (minimum thickness of 6 m), which they suggest may have built up slowly over at least 150 ka. This contrasts to results from seismic investigations of Lake Vostok, the largest of Antarctica's subglacial lakes, which show evidence for a much thicker
80   water column (up to 1100 m) and a thicker layer of lake bottom sediments (up to 400 m) below approximately 4 km of ice (e.g., Filina et al., 2008). Seismic investigations have also been useful for illuminating the properties of subglacial lakes below much thinner ice columns in active ice streams, such as subglacial Lake Whillans which is situated below approximately 800 m of ice and has a maximum water column thickness of less than 10 m (e.g., Horgan et al., 2012).

85   **2 Methods**

2.1 Field experiment

    In June 2018, we conducted a geophysical survey in northwestern Greenland above the candidate subglacial lake feature named "L2" by Palmer et al. (2013). This feature sits within a 980 km^2 drainage basin, is roughly adjacent (< 10 km) to the nearest ice divide (Fig. 1A and 1B), and within an accumulation area. Using RACMO2 1-km resolution modeling of Greenland's near
90   surface climate and surface mass balance (Noel et al., 2018), we estimate the mean annual air temperature to be -22° C. This model is forced with ERA-Interim reanalysis climate information (Dee et al., 2011) at the boundaries and evaluated with in situ observations. The mean annual snow accumulation rate at the field site is ~30 cm/yr ice equivalent. In order to confirm the presence of the subglacial lake and investigate its physical properties, we collected data using both active source seismology and ground-penetrating radio-echo sounding (GPR).

95

The active source seismic experiment (Fig. 1C) consisted of a moving line of 24 40-Hz vertical component geophones spaced 5 m apart. For each line, we collected data at 4 shot locations using an 8 kg sledgehammer impacted against a 1.5 cm thick steel plate. At each source location at least 5 hammer shots were stacked into a single shot gather in order to increase the signal to noise ratio. The first shot location of each line was offset 115 m from the first geophone, and subsequent shot locations were moved 115 m along the line. After data was collected for each of the 4 shot locations, the line was moved 230 m east along the traverse and data collection was repeated. The seismic line was moved a total of 10 times, totalling 40 separate shot locations. Using this geometry, we obtained reflection points at the ice bottom spaced every 2.5 m along a traverse totalling 2400 m (Fig. 1D). We created a seismic reflection image by bandpass filtering data between 100 - 200 Hz and applying a normal moveout (NMO) correction with a velocity of 3700 m/s, which was found to be the average velocity of the ice column from NMO analysis of the primary bed reflection. High frequency spatial noise with wavenumber greater than 0.05 m^{-1} was removed with f-k filtering. Shot gathers with offsets of -115 m and 230 m from the first geophone contained an air wave arrival that was muted by zeroing a 10 ms window with a moveout of 315 m/s.

The GPR data was collected across a ~5.5 km transect roughly parallel to the seismic survey (Fig. 1C), using an acquisition system specially adapted to be towed by a motor sled traveling at approximately 10 km/hr (e.g., Welch & Jacobel, 2003). The system used a Kentech pulse transmitter that produces +/- 2000 V pulses with a variable pulse repetition frequency of between 1 and 5 kHz. The antennae are resistively loaded wire dipoles with nominal frequency of 5MHz, and the receiver uses an 8-bit NI USB-5132 digitizer and a computer. Between 16 and 64 radar shots were stacked were stacked and filtered between 2 - 8MHz to produce each final trace on the radargram. A GPR reflection image was created by converting the radar data to depth using a radar velocity of 172 m/μs (see Supporting Information).

2.2 Basal reflectivity

We calculate the reflection coefficient at the base of the ice by analyzing the amplitudes of the primary bed reflection and its multiple, which we refer to as R1 and R2 from hereon. When both R1 and R2 are visible, the basal reflection coefficient c_R can be determined as a function of incidence angle θ using Eq. (1) where A_{R1} and A_{R2} are the amplitude of the first and second ice bottom reflections, respectively, a is the absorption coefficient, and L is the raypath length of the R1 reflection (e.g., Peters et al., 2008).

$$c_R(\theta) = 2\frac{A_{R2}(\theta)}{A_{R1}(\theta)} e^{aL(\theta)}$$

(1)

At a given geophone, two factors control the amplitude ratio between R1 and R2. First, R1 and R2 reflect off of the lake with slightly different angles, which changes the relative amount of energy partitioned into each reflection. Second, since R2 travels farther than R1, its amplitude is diminished due to geometrical spreading and attenuation. However, at incidence angles in this

study, the difference in reflection coefficients between R1 and R2 is negligible. Additionally, the path lengths of R1 and R2 vary by < 5% between their shortest and farthest offsets. Therefore, to calculate the reflection coefficient c_R we use the normal incidence approximation and compare amplitude ratios A_{R2}/A_{R1} on individual seismograms. In order to minimize the influence of the air wave on A_{R2}/A_{R1} ratio we exclude data from geophones with offsets between 135 – 155 m, where there is potential interference between R1 and the air wave. Measurements of A_{R1} and A_{R2} are made prior to f-k filtering.

The relationship between the absorption coefficient a and the seismic quality factor Q is given by Eq. (2), where c is the seismic velocity, and f is frequency (Bentley & Kohnen, 1976). While in principle, the spectral ratio of the R1 and R2 reflections can be used to determine the attenuation (Q^{-1}) of the glacial ice (Dasgupta & Clark, 1998; Peters et al., 2012) the low signal to noise ratio of the R2 reflection prevents us from making a robust measurement. Here, we estimate the absorption coefficient a based on the study of Peters et al. (2012), who reported Q = 355 +/- 75 in the upper 1 km of ice in Jakobshavn Isbrae, western Greenland. Using Eq. (2) with c = 3.7 km/s, and assuming a frequency of 100 Hz (the predominant frequency observed in the reflections), this corresponds to an absorption factor a = 0.23 +/- 0.06 km^{-1}.

$$Q^{-1} = \frac{ca}{\pi f}$$

(2)

3 Results

The seismic reflection profile (Fig. 2A) shows a clear ice bottom reflection (R1) across the entire transect arriving with a two-way travel time between 400 - 460 ms. The ice bottom multiple R2 (i.e., a wave that has travelled twice between the surface and ice bottom) is also visible between 800 - 920 ms. At transect distances between 0 - 1700 m, the R1 reflection is flat and relatively uniform in character, which we interpret to be the signal of the top of the subglacial lake. In this region, R1 arrives at 457 ms, which corresponds to a depth of 845 m, assuming an average V_P of 3700 m/s within the ice. At larger transect distances, the reflections arrive earlier with increasing distance, which likely reflects the bed topography adjacent to the subglacial lake. An additional reflection is observed arriving between 14 – 20 ms after R1, which we interpret as a lake bottom reflection (Fig. 2B). This signal is intermittently observed but is most continuous at transect distances between 660 – 1200 m. The travel time differential between the lake top and lake bottom reflection is used to measure the thickness of the water column as a function of distance along the transect. Assuming V_P in the lake of 1498 m/s (Table 1), the lake is between 10 – 15 m deep (Fig. 2C). An uncertainty of +/- 50 m/s on lake velocity would correspond to a lake depth uncertainty of +/- 0.5 m. A strong coda following the lake bottom reflection is apparent which is likely caused by a thin (~ 10 m) sediment package underlying the lake (see Discussion).

In the GPR profile, the subglacial lake is apparent as a flat reflector at an elevation of ~510 m along the majority of the transect (Fig. 3A). The surface topography slopes gently to the west across the transect, hence the lake top is slightly deeper (i.e., the ice is thicker) towards the east (Fig. 3B). The lake is beneath 840 m of ice at transect distances between 2 to 4.5 km, which roughly corresponds to the location of the seismic survey. The transition from the lake top to the adjacent bed is observed at approximately 4100 m along the transect. In addition, assuming a uniform two-way englacial attenuation factor of 45 dB/km (as assumed by Palmer et al. (2013) and from analyses similar to MacGregor et al., (2015)), we observe that the reflection amplitudes are approximately 10 dB higher over the lake compared to the surrounding region. However, interpretations are complicated because the thermal profile may vary laterally due to contrasting basal conditions and ice thickness, which has a strong influence on attenuation.

Assuming an absorption factor of $a = 0.23$, the average seismic reflection coefficient of the lake bottom across the transect is -0.43 +/- 0.17 (Fig. 4A). In Fig. 4B, we plot c_R calculated for each shot gather above the lake as a function distance along the transect. For comparison we show the expected reflection coefficients of several different geologic materials underlying glacial ice. Beyond the boundary of the lake, the R2 signal strength is diminished and we are unable to confidently measure c_R. The reflection coefficients were modeled using the two-term approximation of the Zoeppritz equations (e.g., Aki & Richards, 2002; Booth et al., 2015) with the material properties shown in Table 1. In contrast to other likely geological materials at the base of the ice, liquid water is expected to have a strongly negative reflection coefficient. The reflection coefficient modeled for lithified sediments or bedrock underlying ice is similar in amplitude to liquid water but opposite in sign, thus, without polarity information sedimentary rock strata could be mistaken for a lake signature. Here, we measure R1 with an opposite polarity of the source (see Fig. S4), thus, liquid water is the most likely explanation. However, if we are significantly overestimating the magnitude of reflection coefficient, due to for example the large uncertainties on the attenuation structure of the ice, a layer of water saturated dilatant till may also be able to explain our data.

3 Discussion

3.1 Lake geometry and volume

If our interpretation of the observed reflections as signals from the lake top and bottom is correct, it implies that L2 could hold a significant volume of water. Assuming the imaged lake depth of approximately 15 m is representative of average lake depth throughout the roughly 10 km^2 surface area determined by radio-echo sounding, we estimate the total volume of liquid water to be 0.15 km^3 (0.15 Gt of water). While this is only a small fraction of the 217 +/- 32 Gt of ice that Greenland is estimated to lose each year to glacier discharge and surface melting (IMBIE Team Report, 2019), the net storage capacity of all of Greenland's subglacial lakes could be appreciable.

To verify our interpretation of the lake top and bottom reflections, we modeled synthetic seismic waveforms of shot gather 12, which contained some of the clearest reflections. This shot gather corresponds to transect distances between 660 - 720 m in the seismic reflection image. Synthetic seismograms were computed using Specfem2D (Tromp et al., 2008) for two simple layered models of a 12 m thick lake underlying 850 m of glacial ice. In the first model the lake is underlain by a thick layer of sediments that extends to the bottom of the model domain. In the second model there is 10 m of sediments overlying a discontinuity with the bedrock below. The seismic velocity profiles for the two cases are shown in the insets in Fig. 5B and 5C. The source used in the simulations was a Ricker wavelet with a dominant frequency of 100 Hz. Fig. 5 shows a comparison between the observations and synthetics. In both the observed (Fig. 5A) and synthetic (Fig. 5B and 5C) shot gathers, the lake top and lake bottom reflections are separated by ~ 20 ms, and show a clear polarity reversal, which reflects the opposite sign of the acoustic impedance contrast between an ice-water and a water-lake bed transition. The observed shot gather contains a coda following the lake bottom reflection that is absent in the synthetics that do not include a discontinuity at the base of the sediment package (Fig. 5B). When a discontinuity between the sediment and underlying bedrock is included a strong sediment bottom reflection is introduced which more closely matches the observations (Fig. 5C). In the observed data it is difficult to clearly identify a sediment bottom reflection since the complex coda could be caused by reverberations within a thin sediment sequence, or many superposed reflections from individual discontinuities. However, if the first positive peak following the lake bottom reflection represents the base of the sediment, we can estimate a sediment thickness of 8.5 m assuming a sediment V_P of 1700 m/s (Table 1).

3.2 Lake origin

While our results suggest that L2 is indeed a subglacial lake, its presence is perplexing given its location with a mean annual surface temperature of -22º C and its position beneath a relatively thin column of glacial ice. In contrast to many well studied subglacial lakes below Antarctica such as Lake Vostok that lie below ~ 4 km of ice, the basal temperature at our field site is expected to be well below the pressure-dependent melting point of ice. Distinguishing between the different hypotheses of subglacial lake formation has implications for the stability and dynamics of the Greenland ice sheet since they predict different basal thermal and hydrological conditions. Thus, constraining the temperature of L2 is an important goal.

We determine the range of possible basal temperatures using a 1D steady state advection-diffusion heat transfer model solved using the control volume method (see Supporting Information). The modeling assumes an ice density ρ = 920 kg/m³, a heat capacity c_P= 2000 J/kg/K, and a thermal conductivity of ice of k = 2.3 W/m/K. The basal geothermal heat flux q is varied between 50 – 60 mW/m² , which is consistent with estimates derived from magnetic data (Martos et al., 2018) and thermal isostacy modeling (Artemieva, 2019). Fig. 6 shows results for surface temperatures T_s of -20º C and -22º C and ice-equivalent accumulation rates w ranging from 0 to 0.3 m/yr ice equivalent. When vertical advection is ignored (i.e., no ice accumulation), most scenarios predict frozen bed conditions with the exception of the relatively warm surface condition ($T_s = -20º$ C) and high heat flow ($q = 60$ mW/m²) scenario (Fig. 6A). When ice accumulation is considered, all scenarios predict frozen bed

conditions (Fig. 6B). For an ice- equivalent accumulation rate of 0.3 m/yr, which most closely matches the conditions of the field site, and regional average geothermal flux the basal temperature is expected to be between approximately -12°C and -14°C.

There are several possible explanations for the existence of liquid water underneath ice, including hypersalinity, recharge by surface meltwater, high geothermal flux, and latent heat from freezing. Here, we review these explanations and assess their specific relevance to lake L2.

(1) Hypersalinity: If the lake is hypersaline it can remain liquid at low temperatures by depressing the freezing temperature. In order to depress the freezing temperature of water by -12°C to -14°C a NaCl concentration of roughly 160 to 180 ppt would be required, roughly 6x that of seawater (e.g., Fofonoff & Millard Jr, 1983). If the hypersaline condition is restricted to the lake, the surrounding ice would likely be frozen to the bed and would form a closed hydrologic system that could remain isolated on geologic timescales. In this scenario, the lake could represent a body of ancient marine water that was trapped as glacial ice advanced over the area and potentially further enriched in salt through cryogenic concentration processes (Lyons et al., 2005, 2019). Similar hypersaline lakes with salt concentrations several times higher than sea water are known to exist below the McMurdo Dry Valleys in Antarctica (Hubbard et al., 2004; Lyons et al., 2005, 2019; Mikucki et al., 2009) and in the Devon Ice Cap, Canada (Rutishauser et al., 2018). Because the current elevation of the lake is more than 500 m above sea level, it is unlikely to be trapped sea water as in the McMurdo Dry Valleys. While an ancient evaporite deposit is possible, as is proposed for the Devon Ice Cap (Rutishauser et al., 2018), the geologic map of Greenland does not indicate likely evaporites in this area (Dawes, 2004).

(2) Surface meltwater: The lake may be part of an open hydrological system that is continually recharged by surface meltwater. If the hydrological system is connected and the rate of recharge matches or exceeds the rate of freezing, a lake could persist despite sub-freezing temperatures in the lower part of the ice. At other locations in Greenland, observations of vertical surface deformation and collapse features have suggested that surface meltwater plays a prominent role in subglacial lake formation and dynamics (Palmer et al., 2015; Willis et al., 2015). This lake, however, is in the high elevation accumulation area of the ice sheet, near the ice divide (Fig. 1B) and there are no obvious sources for significant surface recharge visible on the ground or from satellite imagery. To determine possible pathways for surface recharge from more distant feature, we estimate the local hydraulic head based on surface and bed elevations (Fig. S5) and find no pathways given the present resolution of bed and surface topography. It is possible that a subglacial pathway exists that is smaller than the resolution of BedMachine (Morlighem et al., 2017).

(3) High geothermal flux: Anomalously high basal heat flux may promote melting of the ice sheet from below (e.g. Fahnestock et al. 2001; Rogozhina et al., 2016). If this is the case, the local geothermal heat flux must greatly exceed regional estimates

of the geothermal heat flux beneath the northwestern Greenland ice sheet, which are typically in the range of 50 – 60 mW/m^2 (Artemieva, 2019; Martos et al., 2018; Rogozhina et al., 2016). Based on the one-dimensional model shown in Fig. 6, a

255   geothermal flux on the order of 100 mW/m^2 would be necessary to sustain the lake. While high heat flux in this region is unexpected based on the cratonic bedrock geology and lack of recent volcanism, a local region of high heat flux could be promoted by the presence of upper crustal granitoids rich in radiogenic heat producing elements or hydrothermal fluid migration through pre-existing fault systems (e.g., Jordan et al., 2018).

260   (4) Latent heat from freezing. For the isolated lake of actively freezing brine (as in Hypothesis 1), the hydrologically connected continuous flow (Hypothesis 2), or if the lake is a relic of a larger freshwater body that is slowly freezing, the thermal profile of the ice would show a curvature change at depth due to a latent heat source at the bottom boundary. Given a latent heat of freezing of 334 J/g, freezing a layer 1 m thick to the bottom of the ice over one year is roughly equivalent to increasing the geothermal flux by 10 mW/m^2.

265

Sustaining a freezing rate of several m/yr to generate the latent heat necessary to maintain warm basal ice is less likely than locally elevated geothermal anomaly. We, therefore narrow the lake origin hypotheses to either anomalously high geothermal flux or hypersalinity due to local ancient evaporite. Measuring the thermal profile and vertical velocity and strain rates above this lake would provide important information to assess these hypotheses. For a freshwater lake created by high geothermal

270   flux, the basal ice temperature would be near 0° C, vertical velocity would be downward (due to melting). For a lake created by evaporite, the basal ice would be substantially below zero, the vertical velocity would be near zero or upward (due to freezing). A geothermally created lake would show higher vertical strain rates in the lower part of the ice column than an evaporite-created lake.

275   A freshwater lake and a hypersaline lake have different physical properties and thus may have different signatures that could be detected in geophysical surveys. Radar reflections from an ice/brine boundary undergoing freezing and cryoconcentration of the brine is known to cause scattering and decrease the reflectivity (Badgeley et al., 2017) which we do not see in our data; this provides a second justification to rule out modern active cryoconcentration; in addition, sustained freezing of any ice is likely to create a radar-detectable basal ice unit such as suggested by Bell et al., (2014).

280

Further, because the seismic velocity and density of water depends on temperature and salinity, we would expect that lakes formed by different mechanisms would have slightly different basal reflection coefficients, although the small variations expected in c_R would not be resolvable with our dataset. On the other hand, because the electrical resistivity of water is strongly dependent on salinity, magnetic sounding could provide useful constraints on lake composition. Additionally, since radar

285   attenuation is strongly sensitive to lake conductivity, radio-echo sounding amplitude data could potentially help constrain salinity if lake bed returns are observed in shallow areas. Stronger constraints could potentially be placed on subglacial

properties if a stronger active source were used (e.g., explosives), since high signal to noise ratio data could be recorded at larger distances. This would be particularly useful for measuring the basal reflectivity as a function of incidence angle, which would help verify our interpretation of a subglacial lake. Repeated seismic reflection or GPR surveys calculated along the same transect could provide clues into whether or not lake levels are changing over time (e.g., Church et al., 2020). Finally, direct sampling with drilling would provide the best measurements on subglacial lake properties and could also yield useful biological and paleoenvironmental information.

4 Conclusions

We conducted an active source seismic reflection and GPR survey in northwestern Greenland above a site that was previously identified as a possible subglacial lake. We observed a horizontal reflector across the majority survey with a seismic reflection coefficient of -0.43 +/- 0.17, consistent with the presence of a lake below approximately 830 – 845 m of ice. Additionally, we observed a lake bottom reflection near the center of our seismic profile consistent with a lake depth of approximately 15 m. From previous observations of the lateral extent of the lake based on airborne radio-echo sounding (Palmer et al. 2013), we estimate the subglacial lake holds a total of 0.15 Gt of water. Strong coda arriving after the lake-bottom reflection suggests that the lake is underlain by a sedimentary package but its thickness and material properties are uncertain. To the authors knowledge, this is the first time a ground-based geophysical survey has confirmed the existence of a subglacial lake in Greenland and provided constraints on its depth. Understanding the nature and origins of recently detected subglacial lakes in Greenland is important since wet basal conditions enable glacial ice to flow more easily which can further promote ice loss. Our analysis of the seismic, radar, as well as thermal and hydropotential analysis narrow the lake origins to either locally high geothermal flux or an ancient evaporite deposit. Future work, such as additional geophysical investigations or drilling expeditions, should focus on constraining the temperature and salinity of the lake which will provide clues to its origin.

Acknowledgements

Funding for this work was provided by the NASA Planetary Science and Technology Through Analog Research (PSTAR) Grant Number 80NSSC17K0229. The authors thank SIIOS (Seismometer to Investigate Icy Ocean Worlds) team members Chris Carr and Renee Weber for helpful discussions. Additionally, we thank editor Evgeny Podolskiy, two anonymous reviewers, and Jacob Buffo for feedback that helped improve this study. Logistical support for field work in northwestern Greenland was provided by Susan Detweiler.

References

Achberger, A. M., Christner, B. C., Michaud, A. B., Priscu, J. C., Skidmore, M. L., Vick-Majors, T. J., & the WISSARD

Science Team. (2016). Microbial community structure of subglacial Lake Whillans, West Antarctica. *Frontiers in Microbiology*, *7*, 1–13. https://doi.org/10.3389/fmicb.2016.01457

Aki, K., & Richards, P. G. (2002). *Quantitative seismology*. University Science Books.

Artemieva, I. M. (2019). Lithosphere thermal thickness and geothermal heat flux in Greenland from a new thermal isostasy method. *Earth-Science Reviews*, *188*(August 2018), 469–481. https://doi.org/10.1016/j.earscirev.2018.10.015

Badgeley, J. A., Pettit, E. C., Carr, C. G., Tulaczyk, S., Mikucki, J. A., & Lyons, W. B. (2017). An englacial hydrologic system of brine within a cold glacier: Blood Falls, McMurdo Dry Valleys, Antarctica. *Journal of Glaciology*, *63*(239), 387–400. https://doi.org/10.1017/jog.2017.16

Bell, R. E., Studinger, M., Shuman, C. A., Fahnestock, M. A., & Joughin, I. (2007). Large subglacial lakes in East Antarctica at the onset of fast-flowing ice streams. *Nature*, *445*(7130), 904–907. https://doi.org/10.1038/nature05554

Bell, R. E., Tinto, K., Das, I., Wolovick, M., Chu, W., Creyts, T. T., … Paden, J. D. (2014). Deformation, warming and softening of Greenland's ice by refreezing meltwater. *Nature Geoscience*, *7*(7), 497–502. https://doi.org/10.1038/ngeo2179

Bentley, C. R., & Kohnen, H. (1976). Seismic refraction measurements of internal friction in Antarctic ice. *Journal of Geophysical Research*, *81*(8), 1519–1526. https://doi.org/10.1029/jb081i008p01519

Bentley, M. J., Christoffersen, P., Hodgson, D. A., Smith, A. M., Tulaczyk, S., & Le Brocq, A. M. (2011). Subglacial Lake Sediments and Sedimentary Processes: Potential Archives of Ice Sheet Evolution, Past Environmental Change, and the Presence Of Life. In *Antarctic Subglacial Aquatic Environments* (pp. 83–110). https://doi.org/10.1002/9781118670354.ch6

Booth, A. D., Emir, E., & Diez, A. (2015). Approximations to seismic AVA responses: Validity and potential in glaciological applications. *Geophysics*, *81*(1), WA1–WA11. https://doi.org/10.1190/geo2015-0187.1

Bowling, J. S., Livingstone, S. J., Sole, A. J., & Chu, W. (2019). Distribution and dynamics of Greenland subglacial lakes. *Nature Communications*, *10*(1), 1–11. https://doi.org/10.1038/s41467-019-10821-w

Campen, R., Kowalski, J., Lyons, W. B., Tulaczyk, S., Dachwald, B., Pettit, E., … Mikucki, J. A. (2019). Microbial diversity of an Antarctic subglacial community and high-resolution replicate sampling inform hydrological connectivity in a polar desert. *Environmental Microbiology*, *21*(7), 2290–2306. https://doi.org/10.1111/1462-2920.14607

Church, G., Grab, M., Schmelzbach, C., Bauder, A., & Maurer, H. (2020). Monitoring the seasonal changes of an englacial conduit network using repeated ground-penetrating radar measurements. *Cryosphere*, *14*(10), 3269–3286. https://doi.org/10.5194/tc-14-3269-2020

Dasgupta, R., & Clark, R. A. (1998). Estimation of Q from surface seismic reflection data. *Geophysics*, *63*(6), 2120–2128. https://doi.org/10.1190/1.1444505

Dawes, P. R. (2004). Explanatory notes to the geological map of Greenland, 1: 500 000, Humboldt Gletscher, Sheet 6. *Geological Survey of Denmark and Greenland (GEUS) Bulletin*, 1–48.

Dee, D. P., Uppala, S. M., Simmons, A. J., Berrisford, P., Poli, P., Kobayashi, S., … Vitart, F. (2011). The ERA-Interim

350 reanalysis: Configuration and performance of the data assimilation system. *Quarterly Journal of the Royal Meteorological Society*, *137*(656), 553–597. https://doi.org/10.1002/qj.828

Fahnestock, M., Abdalati, W., Joughin, I., Brozena, J., & Gogineni, P. (2001). High geothermal heat flow, basal melt, and the origin of rapid ice flow in central Greenland. *Science*, *294*(5550), 2338–2342. https://doi.org/10.1126/science.1065370

Filina, I. Y., Blankenship, D. D., Thoma, M., Lukin, V. V., Masolov, V. N., & Sen, M. K. (2008). New 3D bathymetry and
355 sediment distribution in Lake Vostok: Implication for pre-glacial origin and numerical modeling of the internal processes within the lake. *Earth and Planetary Science Letters*, *276*(1–2), 106–114. https://doi.org/10.1016/j.epsl.2008.09.012

Fofonoff, N. P., & Millard Jr, R. C. (1983). Algorithms for the computation of fundamental properties of seawater. *UNESCO Technical Papers in Marine Sciences*. https://doi.org/http://hdl.handle.net/11329/109

Fricker, H. A., Scambos, T., Bindschadler, R., & Padman, L. (2007). An Active Subglacial Water System in West Antarctica
360 Mapped from Space. *Science*, *315*, 1544–1548. https://doi.org/10.1210/jcem-10-10-1361

Horgan, H. J., Anandakrishnan, S., Jacobel, R. W., Christianson, K., Alley, R. B., Heeszel, D. S., … Walter, J. I. (2012). Subglacial Lake Whillans - Seismic observations of a shallow active reservoir beneath a West Antarctic ice stream. *Earth and Planetary Science Letters*, *331–332*, 201–209. https://doi.org/10.1016/j.epsl.2012.02.023

Hubbard, A., Lawson, W., Anderson, B., Hubbard, B., & Blatter, H. (2004). Evidence for subglacial ponding across Taylor
365 Glacier, Dry Valleys, Antarctica. *Annals of Glaciology*, *39*, 79–84. https://doi.org/10.3189/172756404781813970

Jordan, T. A., Martin, C., Ferraccioli, F., Matsuoka, K., Corr, H., Forsberg, R., … Siegert, M. (2018). Anomalously high geothermal flux near the South Pole. *Scientific Reports*, *8*(1), 1–8. https://doi.org/10.1038/s41598-018-35182-0

Jordan, T. M., Cooper, M. A., Schroeder, D. M., Williams, C. N., Paden, J. D., Siegert, M. J., & Bamber, J. L. (2017). Self-affine subglacial roughness: Consequences for radar scattering and basal water discrimination in northern Greenland.
370 *Cryosphere*, *11*(3), 1247–1264. https://doi.org/10.5194/tc-11-1247-2017

Langley, K., Kohler, J., Matsuoka, K., Sinisalo, A., Scambos, T., Neumann, T., … Albert, M. (2011). Recovery Lakes, East Antarctica: Radar assessment of sub-glacial water extent. *Geophysical Research Letters*, *38*(5), 1–5. https://doi.org/10.1029/2010GL046094

Lyons, W. B., Mikucki, J. A., German, L. A., Welch, K. A., Welch, S. A., Gardner, C. B., … Dachwald, B. (2019). The
375 Geochemistry of Englacial Brine From Taylor Glacier, Antarctica. *Journal of Geophysical Research: Biogeosciences*, *124*(3), 633–648. https://doi.org/10.1029/2018JG004411

Lyons, W. B., Welch, K. A., Snyder, G., Olesik, J., Graham, E. Y., Marion, G. M., & Poreda, R. J. (2005). Halogen geochemistry of the McMurdo dry valleys lakes, Antarctica: Clues to the origin of solutes and lake evolution. *Geochimica et Cosmochimica Acta*, *69*(2), 305–323. https://doi.org/10.1016/j.gca.2004.06.040

380 MacGregor, J. A., Fahnestock, M. A., Catania, G. A., Aschwanden, A., Clow, G. D., Colgan, W. T., … Seroussi, H. (2016). A synthesis of the basal thermal state of the Greenland Ice Sheet. *Journal of Geophysical Research: Earth Surface*, *121*(7), 1328–1350. https://doi.org/10.1002/2015JF003803

MacGregor, J. A., Li, J., Paden, J. D., Catania, G. A., Clow, G. D., Fahnestock, M. A., … Stillman, D. E. (2015). Radar

attenuation and temperature within the Greenland Ice Sheet. *Journal of Geophysical Research: Earth Surface*, *120*, 983–1008. https://doi.org/10.1002/2014JF003418

Martos, Y. M., Jordan, T. A., Catalán, M., Jordan, T. M., Bamber, J. L., & Vaughan, D. G. (2018). Geothermal Heat Flux Reveals the Iceland Hotspot Track Underneath Greenland. *Geophysical Research Letters*, *45*(16), 8214–8222. https://doi.org/10.1029/2018GL078289

Mikucki, J. A., Pearson, A., Johnston, D. T., Turchyn, A. V, Farquhar, J., Schrag, D. P., … Lee, P. A. (2009). A Contemporary Microbially Maintained Subglacial Ferrous "Ocean." *Science*, *663*(5925), 397–401.

Morlighem, M., Williams, C. N., Rignot, E., An, L., Arndt, J. E., Bamber, J. L., … Zinglersen, K. B. (2017). BedMachine v3: Complete Bed Topography and Ocean Bathymetry Mapping of Greenland From Multibeam Echo Sounding Combined With Mass Conservation. *Geophysical Research Letters*, *44*(21), 11,051-11,061. https://doi.org/10.1002/2017GL074954

Palmer, S. J., Dowdeswell, J. A., Christoffersen, P., Young, D. A., Blankenship, D. D., Greenbaum, J. S., … Siegert, M. J. (2013). Greenland subglacial lakes detected by radar. *Geophysical Research Letters*, *40*, 6154--6159. https://doi.org/10.1002/2013GL058383

Palmer, S. J., Mcmillan, M., & Morlighem, M. (2015). Subglacial lake drainage detected beneath the Greenland ice sheet. *Nature Communications*, *6*. https://doi.org/10.1038/ncomms9408

Peters, L. E., Anandakrishnan, S., Alley, R. B., & Voigt, D. E. (2012). Seismic attenuation in glacial ice: A proxy for englacial temperature. *Journal of Geophysical Research: Earth Surface*, *117*(2), 1–10. https://doi.org/10.1029/2011JF002201

Peters, L. E., Anandakrishnan, S., Holland, C. W., Horgan, H. J., Blankenship, D. D., & Voigt, D. E. (2008). Seismic detection of a subglacial lake near the South Pole, Antarctica. *Geophysical Research Letters*, *35*(23), 1–5. https://doi.org/10.1029/2008GL035704

Robin, G., Q., Swithinbank, C. W. M., & Smith, B. M. E. (1970). Radio echo exploration of the Antarctic ice sheet. *International Symposium on Antarctic Glacial Exploration (ISAGE)*, *15*(86), 97--115. https://doi.org/10.1017/s0032247400061143

Rogozhina, I., Petrunin, A. G., Vaughan, A. P. M., Steinberger, B., Johnson, J. V., Kaban, M. K., … Koulakov, I. (2016). Melting at the base of the Greenland ice sheet explained by Iceland hotspot history. *Nature Geoscience*, *9*(5), 366–369. https://doi.org/10.1038/ngeo2689

Rutishauser, A., Blankenship, D. D., Sharp, M., Skidmore, M. L., Greenbaum, J. S., Grima, C., … Young, D. A. (2018). Discovery of a hypersaline subglacial lake complex beneath Devon Ice Cap, Canadian Arctic. *Science Advances*, *4*(4), 1–7. https://doi.org/10.1126/sciadv.aar4353

Siegert, M. J., Dowdeswell, J. A., Gorman, M. R., & McIntyre, N. F. (1996). An inventory of Antarctic sub-glacial lakes. *Antarctic Science*, *8*(3), 281–286. https://doi.org/10.1017/S0954102096000405

Siegfried, M. R., & Fricker, H. A. (2018). Thirteen years of subglacial lake activity in Antarctica from multi-mission satellite altimetry. *Annals of Glaciology*, *59*(76pt1), 42–55. https://doi.org/10.1017/aog.2017.36

Siegfried, M. R., Fricker, H. A., Carter, S. P., & Tulaczyk, S. (2016). Episodic ice velocity fluctuations triggered by a subglacial

flood in West Antarctica. *Geophysical Research Letters*, *43*(6), 2640–2648. https://doi.org/10.1002/2016GL067758

Smith, A. M., Woodward, J., Ross, N., Bentley, M. J., Hodgson, D. A., Siegert, M. J., & King, E. C. (2018). Evidence for the long-term sedimentary environment in an Antarctic subglacial lake. *Earth and Planetary Science Letters*, *504*, 139–151. https://doi.org/10.1016/j.epsl.2018.10.011

Smith, B. E., Fricker, H. A., Joughin, I. R., & Tulaczyk, S. (2009). An inventory of active subglacial lakes in Antarctica detected by ICESat (2003–2008). *Journal of Glaciology*, *55*(192), 573–595. https://doi.org/10.3189/002214309789470879

Stearns, L. A., Smith, B. E., & Hamilton, G. S. (2008). Increased flow speed on a large east antarctic outlet glacier caused by subglacial floods. *Nature Geoscience*, *1*(12), 827–831. https://doi.org/10.1038/ngeo356

The IMBIE Team. (2019). Mass balance of the Greenland Ice Sheet from 1992 to 2018. *Nature*. https://doi.org/10.1038/s41586-019-1855-2

Tromp, J., Komatitsch, D., & Liu, Q. (2008). Spectral-element and adjoint methods in seismology. *Communications in Computational Physics*, *3*(1), 1–32.

Vick-Majors, T. J., Mitchell, A. C., Achberger, A. M., Christner, B. C., Dore, J. E., Michaud, A. B., … Tulaczyk, S. (2016). Physiological ecology of microorganisms in subglacial lake whillans. *Frontiers in Microbiology*, *7*(OCT), 1–16. https://doi.org/10.3389/fmicb.2016.01705

Welch, B. C., & Jacobel, R. W. (2003). Analysis of deep-penetrating radar surveys of West Antarctica, US-ITASE 2001. *Geophysical Research Letters*, *30*(8), 1–4. https://doi.org/10.1029/2003GL017210

Willis, M. J., Herried, B. G., Bevis, M. G., & Bell, R. E. (2015). Recharge of a subglacial lake by surface meltwater in northeast Greenland. *Nature*, *518*(7538), 223–227. https://doi.org/10.1038/nature14116

Woodward, J., Smith, A. M., Ross, N., Thoma, M., Corr, H. F. J., King, E. C., … Siegert, M. J. (2010). Location for direct access to subglacial Lake Ellsworth: An assessment of geophysical data and modeling. *Geophysical Research Letters*, *37*(11), 1–5. https://doi.org/10.1029/2010GL042884

Wright, A., & Siegert, M. (2012). A fourth inventory of Antarctic subglacial lakes. *Antarctic Science*, *24*(6), 659–664.

Young, D. A., Schroeder, D. M., Blankenship, D. D., Kempf, S. D., & Quartini, E. (2016). The distribution of basal water between Antarctic subglacial lakes from radar sounding. *Philosophical Transactions of the Royal Society A: Mathematical, Physical and Engineering Sciences*, *374*(2059). https://doi.org/10.1098/rsta.2014.0297
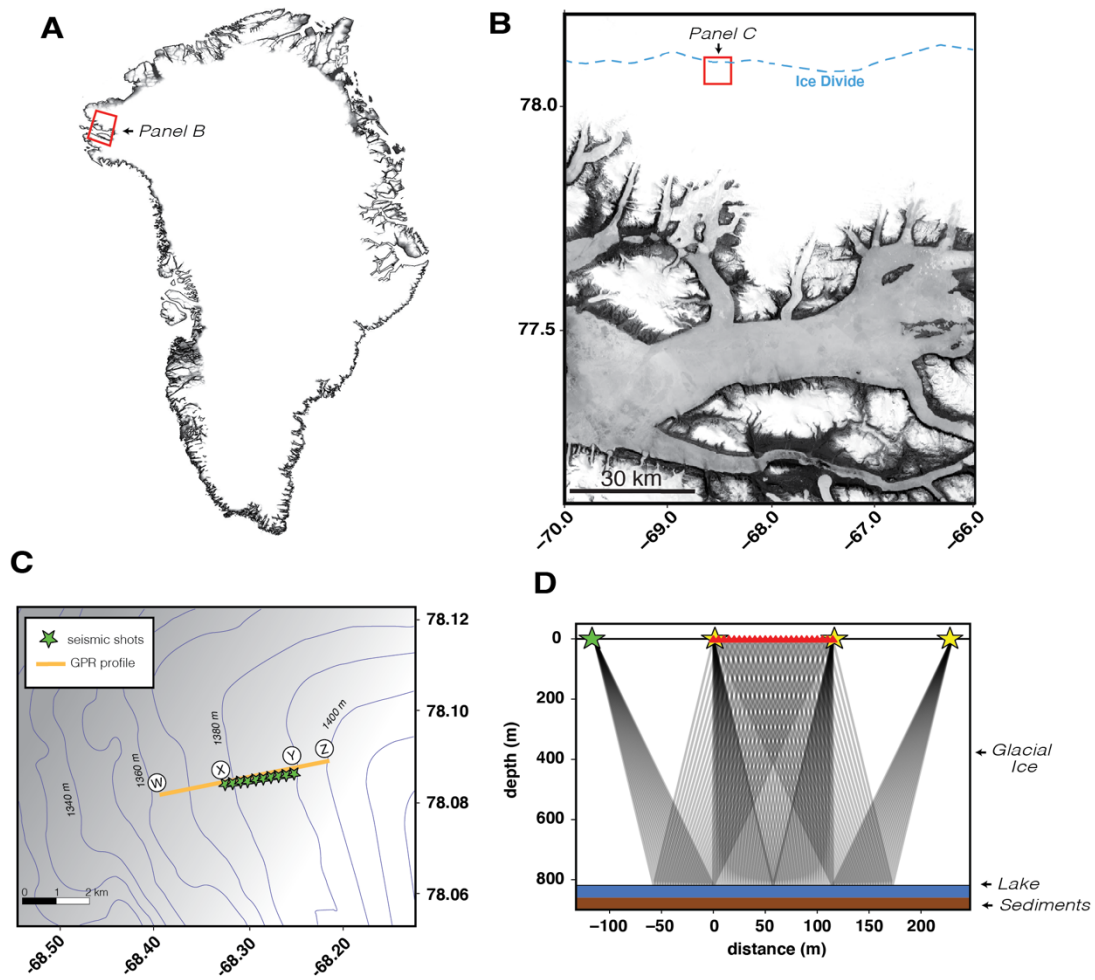
450

Figure 1: (A) Map of Greenland showing our field location in the northwest. **(B)** Composite satellite image from Landsat 8 taken between 2018-5-20 and 2018-5-27. **(C)** Close up map of field region. The green stars show the active source shot and the orange line shows the track of the GPR survey. Only the first of 4 shot locations for each geophone line is plotted. **(D)** Geometry of the active source experiment for a single geophone line. Raypaths of R1 are plotted for all 4 shot locations.

455
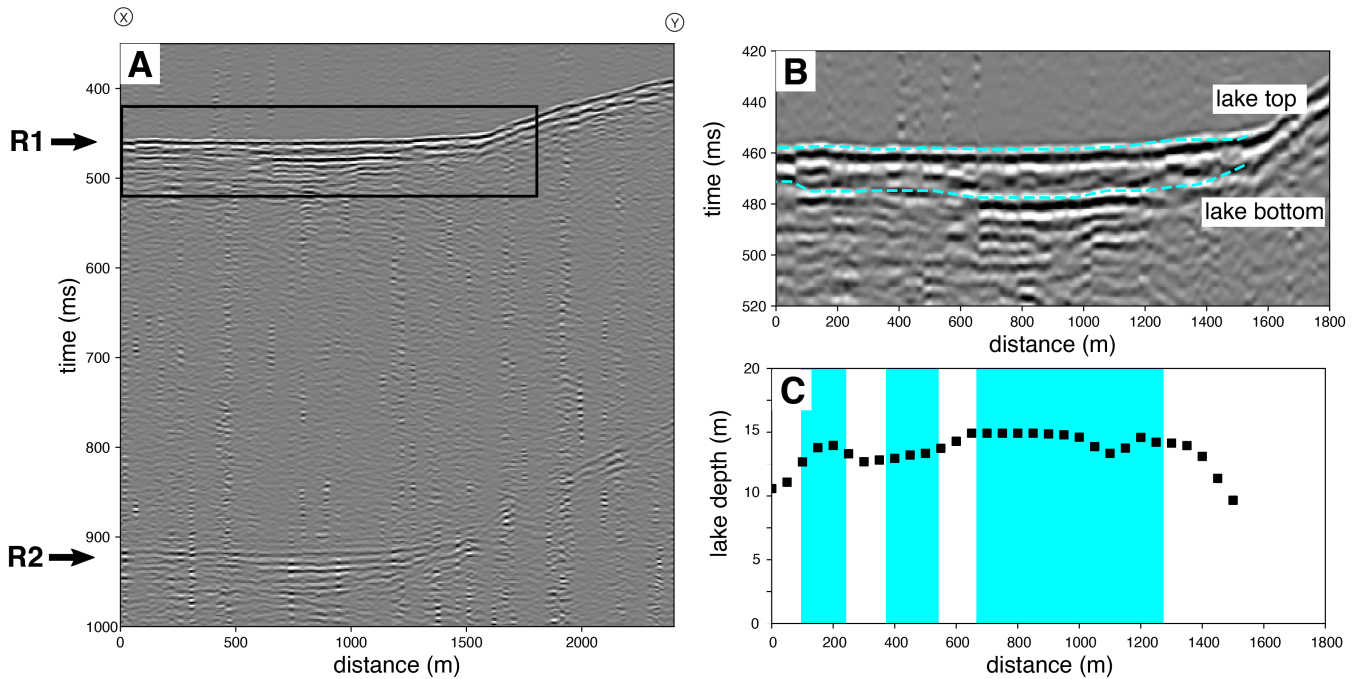
Figure 2. (A) shows the seismic reflection profile of the entire traverse. Reflections labeled R1 and R2 correspond to the primary reflection from the lake top and its multiple. A transect distance of 0 m corresponds to the southwestern end of the line. (B) shows a close up of the R1 reflection window (black rectangle in A), showing reflections from both the lake top and bottom. Travel time picks of the lake top and lake bottom reflections are drawn with the dashed blue line. The depth of the lake inferred from the picked reflections assuming a lake V_P of 1498 m/s is shown in (C). Blue shaded regions indicate where the lake bottom reflection is most clearly identified.

460
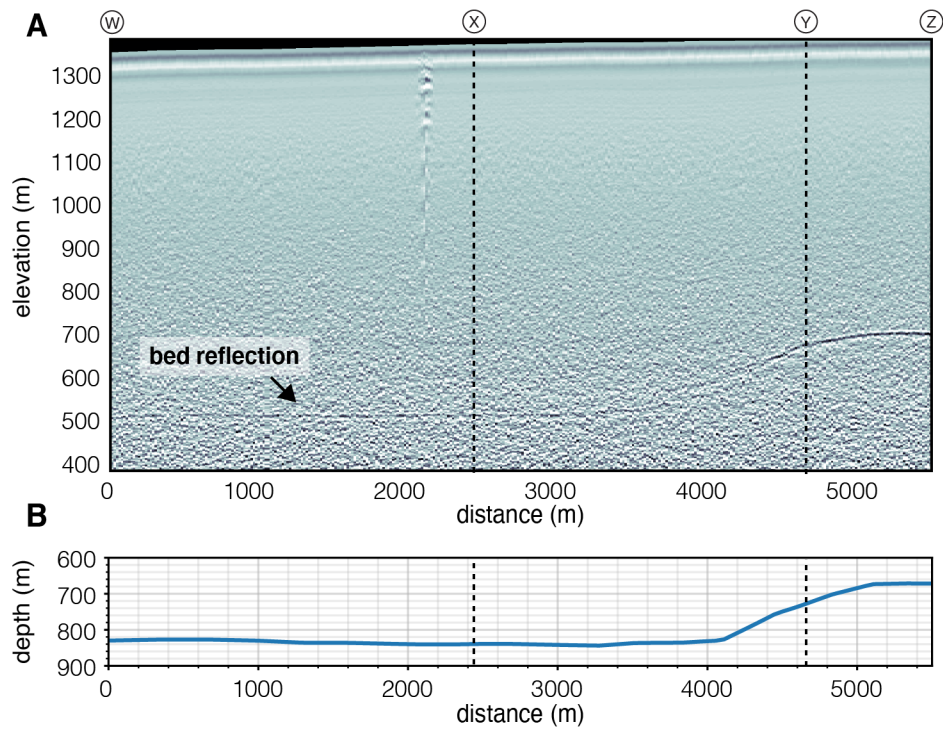
Figure 3. GPR profile. (A) shows the 5 MHz radar data, unmigrated. The primary bed reflection is marked with an arrow. The depth from the surface to the base of the ice is shown in (B). Vertical dashed lines mark the approximate endpoints of the seismic survey.

465

470
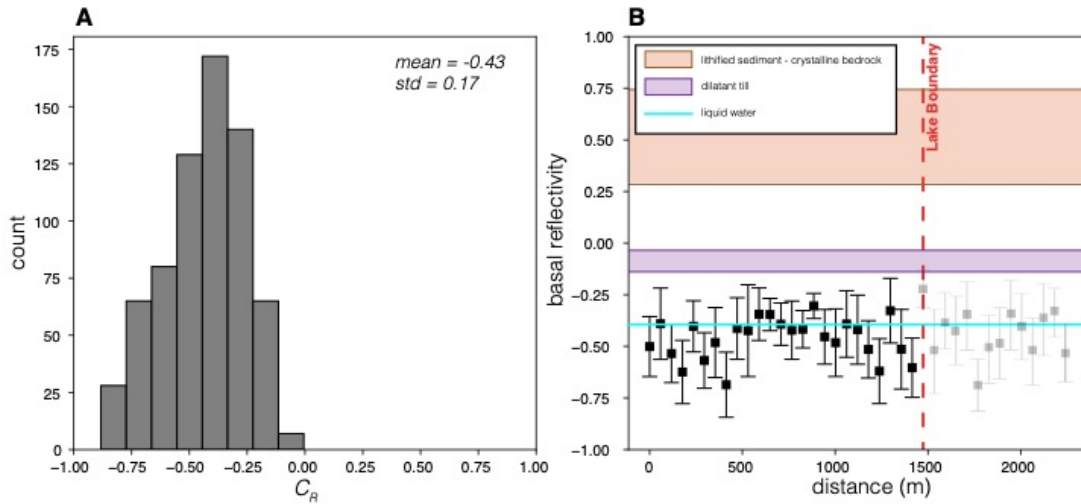
Figure 4. (A) Distribution of reflection coefficients c_R calculated for all shots in the survey. (B) Basal reflectivity as a function of distance along the transect. The black scatter points with error bars show the mean and standard deviation of c_R in a single shot gather, calculated assuming an absorption factor a = 0.23. The shaded regions show the range of expected basal reflectivity values for bedrock or dilatant till and the cyan line shows the basal reflectivity expected for liquid water. The approximate boundary of the subglacial lake is marked by the red dashed line. Values beyond the margin of the lake are shown with light shading because they cannot be confidently interpreted due to the low signal strength of the R2 reflection.
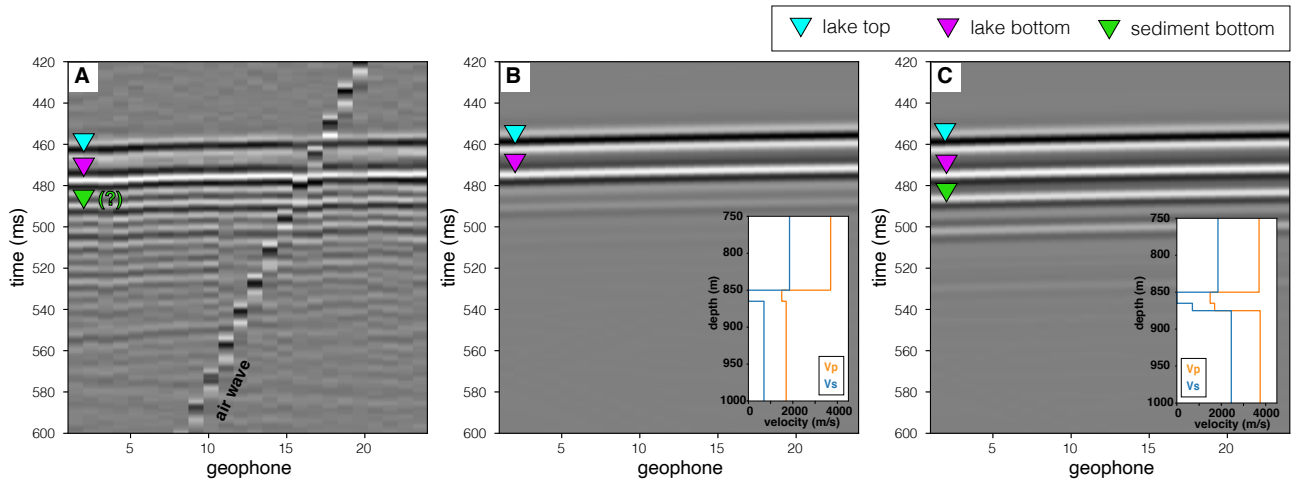
Figure 5. Observed (A) and synthetic (B and C) seismic data for shot gather 12 bandpass filtered between 50 – 200 Hz. The offset from the source to geophone 1 is 230 m. The colored triangles indicate reflections from the lake top (blue), lake bottom (purple), and sediment bottom (green). The insets in panels B and C show the Vp and Vs models that were used to compute the synthetics. Both models include a 12 m thick lake below 850 m of ice. The model used in (C) includes an additional discontinuity 10 m below the lake, which represents the boundary between the lake bottom sediments and underlying bedrock.
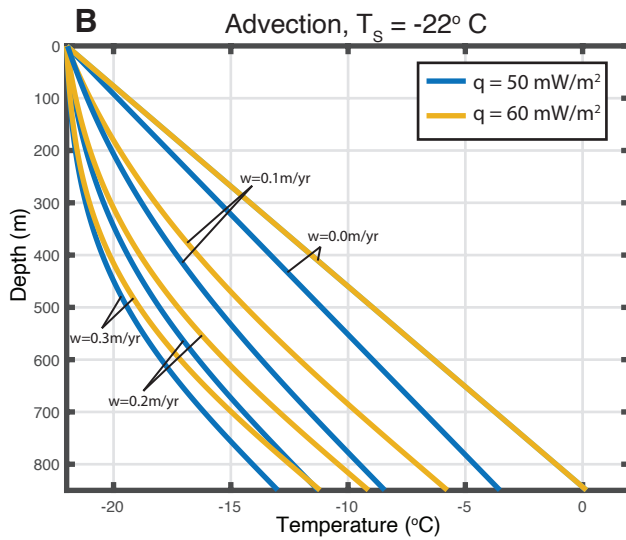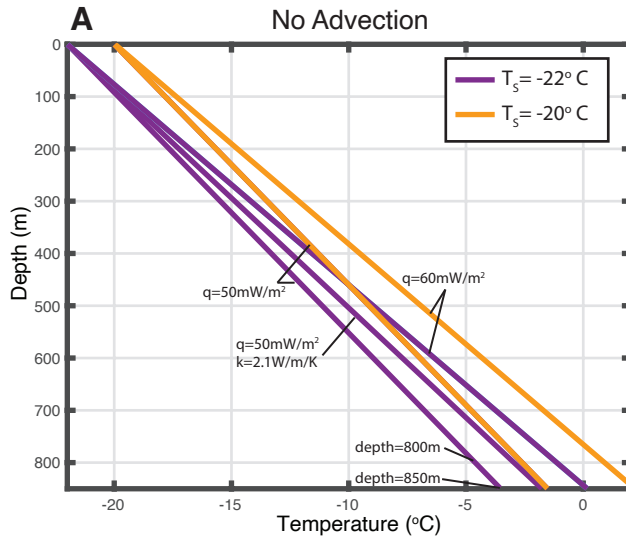
Figure 6. Modeling of ice sheet thermal structure. Panel A shows thermal profiles neglecting advection for surface temperatures T_S = -22° C and T_S = -20° C. Panel B shows thermal profiles including advection for surface temperatures of T_S = -22° C and T_S = -20° C, respectively. The basal heat flux q is varied between 50 – 60 mW/m² and the accumulation rate w is varied between 0 m/yr and 0.3 m/yr.

Material	V_P (m/s)	V_S (m/s)	Density (kg/m^3)
Glacial ice	3810[a]	1860[a]	920[a]
Water	1498[a]	0	1000
Dilatant sediment	1600 –1800[b]	100 – 500[b]	1600 – 1800[b]
Lithified sediment	3000[b] – 3750[a]	1200[b] – 2450[a]	2200[b] – 2450[a]
Bedrock	5200[a] – 6200[b]	2700[a] – 3400[b]	2700[a] – 2800[b]

Table 1. Description of material properties used in reflection coefficient modeling. Values are compiled from Palmer et al., (2008)[a], and Christianson et al. (2014)[b].